Calculation of the electron momentum density and Compton scattering measurements for

nickel

Calculation of the electron momentum density and Compton scattering measurements for nickel

D L Anastassopoulos†, G D Priftis†, N I Papanicolaou‡, N C Bacalis§ and D A Papaconstantopoulos‖

† Department of Physics, University of Patras, GR-26110 Patras, Greece
‡ Department of Physics, University of Ioannina, PO Box 1186, GR-451 10 Ioannina, Greece
§ Theoretical and Physical Chemistry Institute, National Hellenic Research Foundation, Vas. Constantinou 48, GR-11635 Athens, Greece
‖ Naval Research Laboratory, Washington, DC 20375-5000, USA

Abstract. The [100], [110] and [111] directional Compton profiles of single crystals of nickel have been measured using 59.54 keV ^{241}Am γ-rays at a 170° scattering angle and a well defined scattering vector. The electron momentum distribution and Compton profiles in nickel have also been calculated on the basis of a self-consistent augmented-plane-wave method within the local-density approximation including a correlation correction term. A quantitative comparison between experimental and theoretical directional Compton profiles shows good agreement and reveals some accurate information about the Fermi surface. Excitations due to non-local correlation effects from contributing parts to non-contributing parts of the energy bands are very clearly seen along the [100], [110] and [111] directions. The calculation also reproduces quite well the main features of the observed anisotropies, typically within the experimental error margins, although it slightly overestimates their magnitude.

1. Introduction

Compton scattering, an important technique for investigating the electronic structure of materials, provides a sensitive test of the accuracy of first-principles band-structure calculations and the resulting electron wavefunctions [1–3]. The experimentally deduced quantity is the Compton profile (CP) defined as the projection of the ground-state electron momentum density (EMD) along the scattering vector. In particular, the above experimental method has been applied successfully to study the electronic properties of 3d or 4d transition metals.

In this work we report Compton profile measurements on nickel using 59.54 keV γ-rays from a ^{241}Am source along the [100], [110] and [111] directions. It is very interesting to perform such measurements because of the technological importance of nickel and the limited number of reported measurements [4, 5] for Ni single crystals.

Although the efforts on CP measurements are usually concentrated on improving the spectrometer resolution and the statistical accuracy, it would be more important, at least for monocrystals, to ensure a scattering vector k which is very well fixed in space. This

we achieved as explained in section 2, with a result to obtain a geometrical resolution two to four times better than other reported geometrical resolutions [4, 5] while our total resolution is the best reported for an Am spectrometer. This results in a smaller asymmetry in the final CPs and, as we shall see, reveals some information not observed by others [4, 5].

Our main purpose is to present CP anisotropies since these are more sensitive than the absolute CPs when comparing with theory. However, since our CP measurements are equally, if not more, reliable than those of others [5] using an Au source, we deduced the CPs themselves as explained in section 2, and compared them with the calculated profiles in figure 4. We also present a new calculation of the EMD and CPs for the same metal using the self-consistent augmented-plane-wave method (APW) within the local-density approximation of Hedin and Lundqvist [6] in which we included a correlation correction according to Lam and Platzman [7]. Since the theoretical data available above 2.5 au are not sufficient [8], a new calculation is needed.

In a Compton experiment we cannot distinguish between different spin states using conventional x- or γ-rays. Only with polarized x- or γ-rays can we reveal this difference [9]. Consequently a non-magnetic calculation is sufficient for comparisons with this experiment. To check this, we also performed a spin-polarized calculation and compared the spin-up plus spin-down EMD with the non-magnetic value. After convolution, the differences in the CPs are within 0.4% of the total $J(0)$ and the CP anisotropies agree within the experimental errors. Thus the comparisons with experiment are not affected. The same is true for the Lam–Platzman correlation correction term too.

The experimental procedure is described in section 2 and the method of calculation is outlined in section 3. The results of the theoretical EMD and comparisons between calculated and experimental absolute CPs as well as CP anisotropies are presented and discussed in section 4. Conclusions are given in section 5.

2. Experimental procedure

In the present work we attempt detailed measurements of directional CPs for Ni and their anisotropies. These measurements are only useful if the direction of the scattering vector is fixed [1, 10]. There are two reasons leading to a non-fixed scattering vector. One is the inaccuracy in the definition of the scattering angle and the other is the change in the magnitude of the scattered wavevector across the Compton profile. Favourable conditions for a well defined scattering angle are obtained by choosing long distances between the source and the sample and between the sample and the detector while the stability of the scattering vector is improved in the case of a scattering angle close to 180°. However, the application of these favourable conditions leads to a significant reduction in the intensity and consequently a longer measurement time would be required if the statistical errors were to be kept small.

With the above considerations in mind a spectrometer ensuring a scattering vector k which is very well fixed in space was built, consisting of the following characteristics. The collimation system was constructed around a 300 mCi ^{241}Am disc source (12 mm in diameter) determining a scattering angle of 170°.

The angular distribution of the scattering power was obtained by a Monte Carlo calculation. The geometrical divergence of the collimation system was calculated to ±2.1° with a mean scattering angle of 170° and a FWHM of 2° (equivalent to 28 eV of
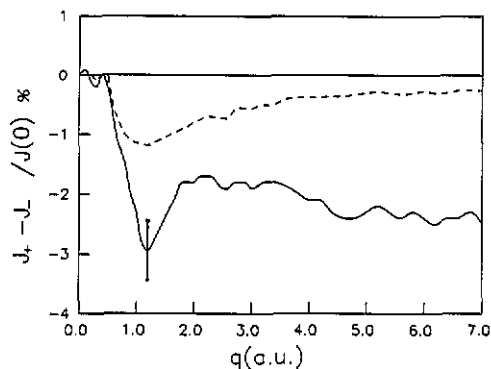
Figure 1. Asymmetry of the experimental CP in the ⟨100⟩ direction before the removal of the low energy tail of the resolution function (————) and after the removal of this energy tail (— — —). In the full curve the influence of non-excited $1s^2$ electrons from 4.4 to 7.0 au has been considered by subtracting their contribution from the low-energy side of the spectrum.

energy spread) [10]. Thus a geometrical resolution Δq of 0.04 au results, which is two to four times better than in other measurements on Ni single crystals [4, 5].

The solid state detector is a Canberra low-energy germanium detector and has a resolution of 357 eV FWHM at 59.54 keV γ-ray energy. The detector has a 100% efficiency for the γ-ray energy of interest. Since the geometrical resolution was negligibly small, the total resolution of the spectrometer was equal to the energy resolution of the detector [10]. This means a resolution of 0.52 au of momentum near the peak of the Compton profile, the best achieved with an Am spectrometer.

The samples used were nickel single crystals cut along the [100], [110] and [111] directions, with a diameter of 2 cm and a thickness of 1.5 mm, 1.2 mm and 1.1 mm, respectively, obtained from Metal Crystals Ltd, Cambridge. The channel width was fixed at 60.5 eV while the drift in the detecting system was found to be less than 0.05 channels at 59.54 keV. About 8×10^4 counts were accumulated at the channel of the Compton peak for a total period of 80 d for each sample. The signal-to-noise ratio was about 160 in the Compton peak region.

Data analysis includes background subtraction, a correction for the energy dependence of the Compton scattering cross section and a calculation of the absorption in the sample [1].

The multiple-scattering contribution to the Compton profile was calculated. Since the ratio of double to single scattering is not simply related to the thickness of the sample, the method of extrapolating to zero thickness is not feasible for a thick sample as in our case. The correction was instead performed by the Monte Carlo method [11]. In this method the intensity and the spectral distribution of double scattering are calculated separately, resulting in a great reduction in computing time. The ratio of double to single scattering was calculated to be 9.8% when 10 000 double-scattering events were generated and 1% accuracy in the above ratio was obtained. This ratio results in a 4% correction at the Compton peak.

The detector response function has a low-energy tail. A similar tail is obtained in the spectrum of the incident beam owing to the source self-absorption. These two effects introduce an asymmetry of 3% in the CP. In order to correct this asymmetry, we measured the spectrum of the resolution function directly from the source, and we used this function to deconvolute the measured spectra. Finally the deconvoluted spectra were smoothed by convolution with only the symmetric part of the resolution function. The asymmetry in the CP before and after the above correction is plotted in figure 1. It should be noted that, compared with the Au experiment on Ni [5] as well as with other

experiments [12], this final asymmetry of ours is smaller, especially for $q > 2$ au. Since the main problem in measuring CPs is the asymmetry encountered, we found that, with a spectrometer having a very well defined scattering vector k, one can obtain reliable absolute CPs [13]. Furthermore, in order to avoid any effect of the asymmetry, the final absolute CPs have been taken only from the high-energy side of the spectrum.

The spectra were normalized to 12.18 electrons from $q = 0$ up to $q = 7$ au, because the $1s^2$ electrons of Ni are not excited in the region from 4.4 to 7.0 au, since their binding energy is greater than the energy transferred. Accordingly from the theoretical CPs the contribution of the $1s^2$ electrons was subtracted.

3. Method of calculation

The computational procedure has already been described elsewhere [14]. Here we give only an outline of the method. The electronic band structure for FCC nickel has been calculated self-consistently by using the symmetrized APW method [15]. Darwin and mass–velocity relativistic corrections have been included and the spin–orbit coupling has been neglected. The exchange and correlation part of the crystal potential was calculated using the local-density approximation of Hedin and Lundqvist [6]. The lattice constant used was $\alpha = 6.6592$ au.

The APW energy values and wavefunctions were calculated on a grid of 89 k-points in one forty-eighth of the first Brillouin zone (BZ).

Within the independent-particle approximation, the EMD $\rho(p)$ for the band electrons at a momentum $p = k + G$ is expressed as

$$\rho(p) = \delta(p - k - G) \sum_{k,j,s}^{occ} \left| \int_{cell} \exp(-ip \cdot r) \, \Psi_{k,j,s}(r) \, d^3r \right|^2 \tag{1}$$

where $\Psi_{k,j,s}(r)$ is the wavefunction of the electron with spin s in a state k in the jth band and G is the reciprocal lattice vector. We have used 537 G-vectors per k-point in momentum space; so the maximum momentum obtained is $p_{max} \approx 8$ au, which is sufficient for the band electrons.

Within the impulse approximation [16] the Compton profile along a direction $\hat{e}$ is related to the momentum density through the expression

$$J(q, \hat{e}) = \int \rho(p)\delta(q - p \cdot \hat{e}) \, d^3p. \tag{2}$$

The calculated band CP obeys the normalization condition

$$\int_{-p_{max}}^{p_{max}} J(q, \hat{e}) \, dq = 10 \tag{3}$$

which is the number of band electrons of Ni per unit cell. Finally, we included the so-called Lam–Platzman [7] correction for the CP of Ni in the local-density approximation using the following expression:

$$\Delta J(q) = \int_{unit\,cell} [J^{int}(\sigma(r); q) - J^{free}(\sigma(r); q)]\sigma(r) \, d^3r \tag{4}$$

where $J^{int} - J^{free}$ is the difference between the CPs of the homogeneous interacting and

non-interacting electron gases with local electronic charge density $\sigma(r)$, both normalized to one electron. This correlation correction term mainly has an effect for low momenta; it is spherically symmetric and thus cancels out in the anisotropies [17]. We used our self-consistent muffin-tin charge density $\sigma(r)$ and the term J^{int} was computed using the occupancy functions of Lundqvist [18]. Details of this computation have been given in [19].

4. Results and discussion

4.1. Electron momentum density

The electron momentum densities for Ni obtained from our calculation are plotted in figures 2(a), 2(b) and 2(c), along the three symmetry directions [100], [110] and [111], respectively. The corresponding energy bands are shown in the insets. According to the selection rule given by Harthoorn and Mijnarends (HM) [20], only the bands Δ_1, Σ_1 and Λ_1 having totally symmetric representations contribute to the total EMD along the [100], [110] and [111] directions, respectively. These bands are labelled (A), (B), etc, in the insets in figure 2; the broken line represents the Fermi energy.

Our theoretical $\rho(p)$ agree qualitatively with earlier results [21] for paramagnetic nickel obtained by employing the approximate method of Hubbard [22] and Mijnarends [23]. The shape of the EMD together with the various features and Fermi breaks can be analysed on the basis of the respective energy bands, the Fermi surface topology and the character of the wavefunctions.

The lowest Δ_1, Σ_1 and Λ_1 bands (labelled A in figures 2(a), 2(b) and 2(c), respectively) are completely occupied and contribute to the total $\rho(p)$ with a smooth behaviour. At low momenta their partial EMD is flat owing to their s-like character. As p increases, these bands lose their s character because of hybridization with the d bands, and the corresponding EMDs decrease rapidly.

Along the [100] direction the next higher Δ_1 band (labelled (B)) in figure 2(a) is partially occupied and its contribution increases slowly as p^4 at very low momenta, since the Γ_{12} level is a pure d state. At $p = 0.5$ au this band hybridizes with the conduction band and changes to an s–p-like character near X_4'. Its momentum density increases rapidly and gives a discontinuity in the total EMD inside the first BZ, when the corresponding band crosses the Fermi level. The Fermi breaks also appear in higher zones via the Umklapp process.

Along the [110] direction, the next higher Σ_1 band (labelled (B) in figure 2(b)) is completely occupied; it is d-like inside the first BZ and gives a broadening of the total $\rho(p)$. In addition, there is a higher Σ_1 band (labelled (C) in figure 2(b)), which is partially occupied and starts with a d-like character. Its contribution is significant between 2.2 and 3.2 au through the Umklapp process.

Finally, along the [111] direction the upper Λ_1 band (labelled (B) in figure 2(c)) has a similar character to that of the upper Δ_1 band but now is completely occupied; thus the total EMD shows a smooth behaviour without Fermi breaks.

4.2. Directional Compton profiles

Our calculated Compton profiles corresponding to the band electrons of nickel are given in table 1 for the symmetry directions [100], [110] and [111]. In comparing the above
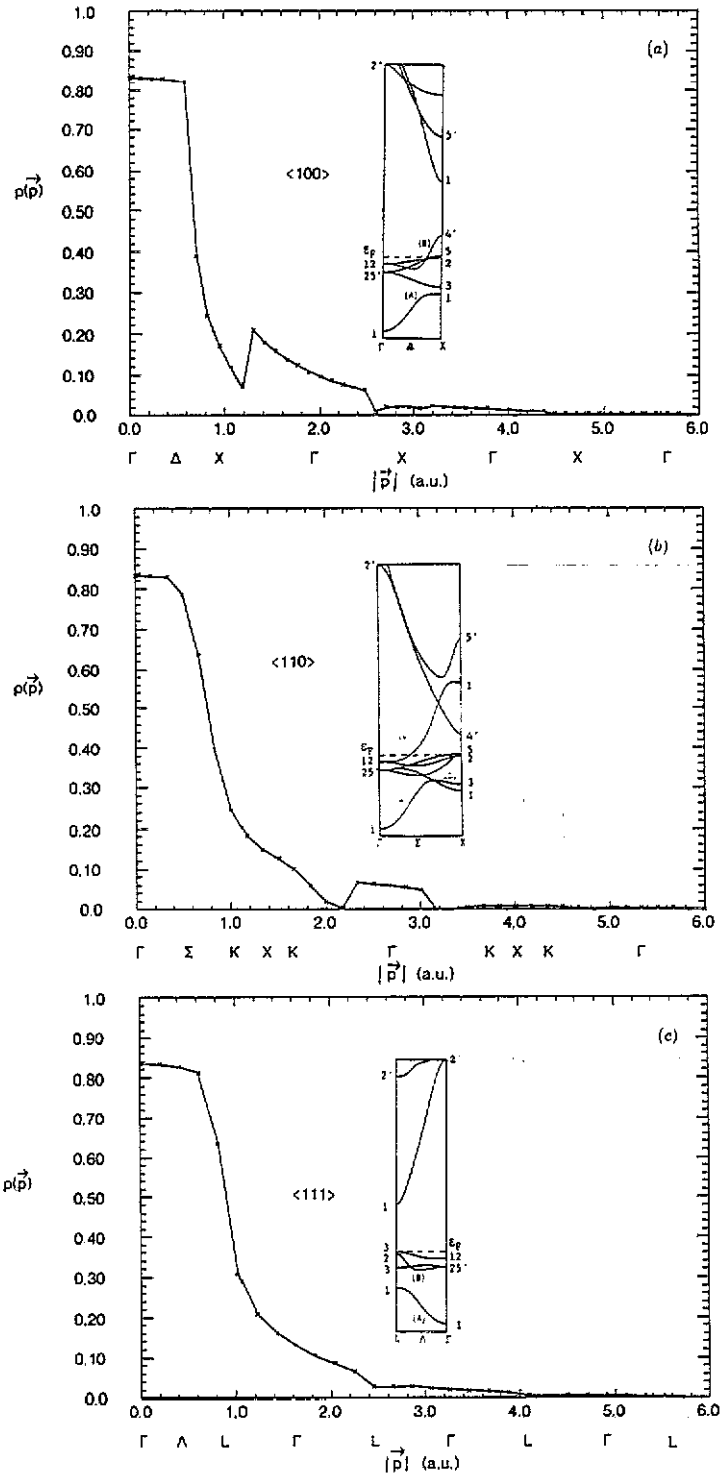
Figure 2. Theoretical electron momentum density of the band electrons of Ni along (*a*) [100], (*b*) [110] and (*c*) [111] directions. (The full curves connect the calculated points.) The insets show the corresponding energy bands.

Table 1. The calculated directional Compton profiles of the valence electrons of nickel, and the Lam–Platzman correction term $\Delta J(q)$.

q (au)	$J(q)$				q (au)	$J(q)$			
	[100]	[110]	[111]	$\Delta J(q)$		[100]	[110]	[111]	$\Delta J(q)$
0.0	2.819	2.766	2.828	−0.045	3.6	0.309	0.297	0.314	0.004
0.1	2.785	2.773	2.785	−0.045	3.7	0.277	0.282	0.281	0.004
0.2	2.786	2.733	2.737	−0.044	3.8	0.260	0.275	0.267	0.004
0.3	2.746	2.677	2.684	−0.043	3.9	0.243	0.271	0.247	0.004
0.4	2.642	2.604	2.567	−0.041	4.0	0.241	0.259	0.236	0.005
0.5	2.498	2.430	2.451	−0.037	4.1	0.224	0.239	0.227	0.005
0.6	2.334	2.227	2.291	−0.033	4.2	0.203	0.215	0.201	0.005
0.7	2.161	2.069	2.115	−0.028	4.3	0.188	0.197	0.186	0.005
0.8	1.964	1.954	1.982	−0.021	4.4	0.178	0.185	0.174	0.005
0.9	1.832	1.870	1.845	−0.010	4.5	0.165	0.164	0.161	0.005
1.0	1.708	1.760	1.740	0.006	4.6	0.144	0.133	0.157	0.005
1.1	1.611	1.694	1.663	0.021	4.7	0.133	0.115	0.140	0.005
1.2	1.559	1.640	1.547	0.019	4.8	0.123	0.116	0.125	0.005
1.3	1.451	1.576	1.465	0.015	4.9	0.118	0.115	0.118	0.005
1.4	1.342	1.471	1.381	0.011	5.0	0.113	0.106	0.107	0.004
1.5	1.277	1.333	1.262	0.008	5.1	0.103	0.100	0.103	0.004
1.6	1.233	1.228	1.213	0.007	5.2	0.094	0.096	0.095	0.004
1.7	1.134	1.144	1.139	0.005	5.3	0.087	0.092	0.082	0.004
1.8	1.019	1.059	1.075	0.004	5.4	0.081	0.085	0.076	0.004
1.9	0.968	0.934	1.059	0.004	5.5	0.071	0.077	0.070	0.004
2.0	0.909	0.833	0.955	0.003	5.6	0.062	0.071	0.065	0.004
2.1	0.907	0.803	0.886	0.003	5.7	0.056	0.065	0.061	0.004
2.2	0.862	0.797	0.846	0.003	5.8	0.051	0.057	0.051	0.003
2.3	0.791	0.770	0.790	0.003	5.9	0.049	0.043	0.046	0.003
2.4	0.735	0.742	0.771	0.003	6.0	0.045	0.031	0.043	0.003
2.5	0.699	0.721	0.716	0.003	6.1	0.040	0.029	0.039	0.003
2.6	0.658	0.705	0.642	0.003	6.2	0.035	0.028	0.036	0.003
2.7	0.581	0.660	0.605	0.004	6.3	0.032	0.024	0.030	0.002
2.8	0.539	0.603	0.558	0.004	6.4	0.028	0.022	0.024	0.002
2.9	0.502	0.550	0.523	0.004	6.5	0.023	0.020	0.022	0.002
3.0	0.483	0.507	0.501	0.004	6.6	0.020	0.019	0.020	0.002
3.1	0.469	0.472	0.441	0.004	6.7	0.016	0.018	0.018	0.002
3.2	0.428	0.403	0.405	0.004	6.8	0.014	0.016	0.014	0.002
3.3	0.389	0.335	0.379	0.004	6.9	0.013	0.015	0.009	0.002
3.4	0.364	0.308	0.349	0.004	7.0	0.010	0.014	0.008	0.001
3.5	0.344	0.305	0.342	0.004					

results with those of an earlier LCGO band-structure calculation [8], we see that, for q between 0.0 and 2.5 au, our values are generally larger than theirs by about 1–3% of $J(0)$ of the valence electrons, while for higher momenta the differences are smaller. This may be due to the different calculation methods and to the different number of reciprocal lattice vectors. In order to make a direct comparison of the calculation with our experimental measurements, we added to the above theoretical values; firstly the Hartree–Fock free atomic core CPs calculated by Biggs *et al* [24] in the momentum region that each contributes and secondly the Lam–Platzman correction term $\Delta J(q)$ given in table 1. Finally, we convoluted these values with a Gaussian of FWHM 0.52 au in order to account for the experimental resolution.
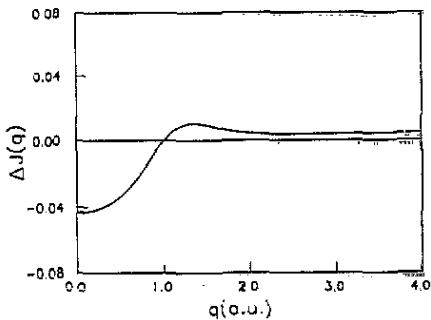
Figure 3. The Lam–Platzman correction term to the theoretical Compton profiles of nickel after convolution with a Gaussian of FWHM 0.52 au.

Figure 3 shows the Lam–Platzman correction to the theoretical CP for Ni after convolution with the experimental resolution. It is obvious that its effect is significant only inside the first BZ and transfers electrons to higher-momentum states.

In table 2 we give for comparison the experimental and theoretical directional CPs of Ni.

Figure 4 shows the differences $J_{exp}(q) - J_{the}(q)$ between the experimental and theoretical CPs for the three orientations in Ni. For all the directions we find a systematic maximum difference of about 2% of $J(0)$, especially for momenta outside the first BZ, since the correlation correction term (figure 3) reduces such discrepancies between theory and experiment mainly in the vicinity of $q = 0$. The oscillatory structure of the difference along the [110] direction (figure 4(b)) also has been found recently by Rollason et al [5], who measured the directional CPs of nickel using 412 keV γ-ray spectrometers and compared their measurements with the LCGO band-structure calculation [8]. This structure arises because the theory shows a larger CP inside and a smaller CP outside the Fermi surface.

The differences between the experimental and the theoretical CPs along the measured directions show two main features. One is that the theoretical values are larger than the experimental values for small momenta, say $q < 1.5$ au. This can be attributed to the normalization of the CP within a limited k-space used in the theoretical calculation. The other is an oscillatory structure mainly at large momenta where the contribution of the s-type electronic states to the EMD has ceased, leaving only the contribution from the d-type states. This structure has not always been seen in other experiments [5] and is, we think, very important because it could reveal accurate information about the Fermi surface by simultaneously testing both the theory and the experiment [17], if it could be explained using the following observations. According to the HM [20] selection rule, only the bands labelled (A), (B) and (C) in the band-structure insets in figure 2 contribute to the EMD. All the highest bands are partially occupied, cutting the Fermi level at some k-point. At this point and at the equivalent points in the repeated zone scheme the EMD curve shows a corresponding jump, indicating clearly where the zone is occupied and where it is not. By looking at the differences between the experimental and the theoretical CPs (figure 4), we see that in the vicinity of the Fermi cut, and on the side of the unoccupied part of the zone, the experiment always shows a larger CP than the theory predicts. This means that there are actually a few electrons partially occupying this part of the zone just above the Fermi level. This can be explained either by thermal excitations or, more important, by non-local correlation effects [17], which both are not accounted for by our theoretical calculation. These electrons are missing from wherever it is the

Table 2. Experimental and theoretical Compton profiles of nickel along [100], [110] and [111] directions. The theoretical values which include the core contribution [24] and the correlation correction term (equation (4)) have been convoluted with a Gaussian of FWHM 0.52 au.

q (au)	Experiment $J(q)$			Theory $J(q)$		
	[100]	[110]	[111]	[100]	[110]	[111]
0.0	5.141	5.130	5.095 ± 0.026	5.186	5.144	5.158
0.1	5.123	5.110	5.077	5.171	5.128	5.141
0.2	5.079	5.056	5.029	5.125	5.078	5.091
0.3	5.001	4.967	4.950	5.048	4.996	5.010
0.4	4.898	4.850	4.843	4.939	4.885	4.900
0.5	4.760	4.709	4.709	4.803	4.750	4.766
0.6	4.600	4.552	4.558	4.644	4.599	4.614
0.7	4.423	4.383	4.385	4.471	4.440	4.450
0.8	4.237	4.212	4.208	4.291	4.281	4.282
0.9	4.047	4.037	4.027	4.110	4.124	4.112
1.0	3.857	3.867	3.850 ± 0.022	3.934	3.971	3.944
1.1	3.676	3.697	3.673	3.763	3.819	3.777
1.2	3.496	3.531	3.502	3.596	3.663	3.612
1.3	3.319	3.364	3.339	3.433	3.503	3.447
1.4	3.156	3.200	3.183	3.271	3.336	3.285
1.5	3.009	3.039	3.035	3.112	3.163	3.125
1.6	2.870	2.884	2.890	2.955	2.989	2.972
1.7	2.739	2.738	2.754	2.803	2.817	2.823
1.8	2.619	2.601	2.636	2.656	2.651	2.680
1.9	2.499	2.473	2.513	2.516	2.495	2.541
2.0	2.379	2.351	2.394 ± 0.017	2.385	2.353	2.407
2.2	2.138	2.125	2.157	2.141	2.111	2.155
2.4	1.903	1.909	1.930	1.916	1.913	1.926
2.6	1.691	1.713	1.720	1.707	1.734	1.719
2.8	1.520	1.544	1.534	1.522	1.557	1.532
3.0	1.380	1.396	1.389 ± 0.013	1.365	1.382	1.367
3.5	1.096	1.092	1.103	1.056	1.037	1.052
4.0	0.878	0.882	0.882	0.839	0.851	0.841
4.5	0.685	0.691	0.682	0.660	0.659	0.660
5.0	0.563	0.563	0.560	0.529	0.525	0.528
5.5	0.465	0.470	0.468	0.443	0.447	0.442
6.0	0.407	0.403	0.404	0.375	0.371	0.374
6.5	0.365	0.366	0.366	0.319	0.316	0.318
7.0	0.304	0.304	0.304	0.272	0.274	0.271

easiest for them to leave, i.e. either from just below the Fermi cut, or from other places in k-space if they are close to the Fermi level. These places always correspond to local minima in figure 4. For example, along the $\langle 100 \rangle$ direction, all minima at 1.4, 2.8, 3.2, 4.4 and 5.4 au correspond to places just below the Fermi cut, and the maximum at 4.8 au corresponds to k-points just above the Fermi cut in the fourth BZ. Along the $\langle 110 \rangle$ direction the minima at 2.7, 5.4 and 6.2 au and the maxima at 2.1, 3.5, 4.8 and 6.6 au correspond to places just below and just above the Fermi cut, respectively, whereas the minima at 1.35 and 4.1 au correspond to places near X_2 which are very close to the Fermi level. Along the $\langle 111 \rangle$ direction there is a large energy gap starting from L_3; so there are not so many places available for the electrons to be excited, except near L, at 0.8, 2.4,
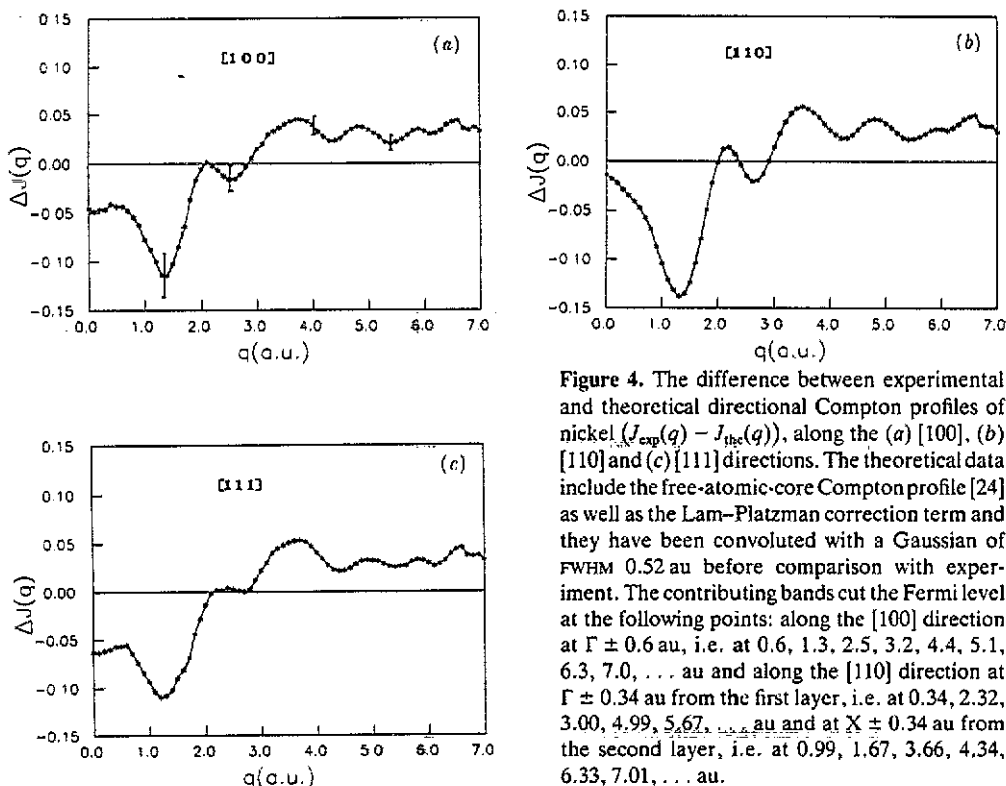
Figure 4. The difference between experimental and theoretical directional Compton profiles of nickel $(J_{exp}(q) - J_{the}(q))$, along the (a) [100], (b) [110] and (c) [111] directions. The theoretical data include the free-atomic-core Compton profile [24] as well as the Lam–Platzman correction term and they have been convoluted with a Gaussian of FWHM 0.52 au before comparison with experiment. The contributing bands cut the Fermi level at the following points: along the [100] direction at $\Gamma \pm 0.6$ au, i.e. at 0.6, 1.3, 2.5, 3.2, 4.4, 5.1, 6.3, 7.0, ... au and along the [110] direction at $\Gamma \pm 0.34$ au from the first layer, i.e. at 0.34, 2.32, 3.00, 4.99, 5.67, ... au and at X $\pm$ 0.34 au from the second layer, i.e. at 0.99, 1.67, 3.66, 4.34, 6.33, 7.01, ... au.

3.8 and 5.8 au, where figure 4(c) shows some maxima, whereas the minima, near the middle of ΓL, at 1.2, 2.8, 4.4 and 5.2 au, are not so strong; so the oscillatory structure is not so regular. The more abrupt the zone near the Fermi cut the easier it can be seen with a small geometrical resolution because there is a wide energy range at that k-point for the electrons to be measured, and because there are no other k-points nearby to smear the data as in the case of a smooth Fermi cut. This is the reason, we believe, that no evident oscillatory structure was seen with a geometrical resolution 400% lower than ours [5] along the ⟨110⟩ and ⟨111⟩ directions. There is also one more case that could produce weak local maxima in figure 4, which should be clearly due to non-local correlation effects; occupied zones forbidden by the HM selection rule may start to contribute to the EMD along a specific direction, if they are nearly degenerate with allowed occupied zones. All maxima not mentioned above in all three curves of figure 4 correspond to such places. This is, we think, the case near $\Gamma_{25'}$ along the ⟨100⟩ and the ⟨111⟩ directions corresponding to the maxima at 2.1, 3.9 and 4.8 au and at 1.5, 3.1 and 4.7 au, respectively. In fact, we would attempt to say that the maximum is weakly but clearly seen just before and just after Γ, but more accurate data would be needed to ensure this. We believe that this should also happen along the ⟨110⟩ direction, but there we have already a deep minimum for the previous reasons, which could cover the weak maximum.

We should notice that the first and main minima near X, along the ⟨100⟩ and ⟨110⟩ directions, and between Γ and L along the ⟨111⟩ direction are also seen but are not mentioned in [5] except that of the ⟨110⟩ direction, which, we believe, is due to X and
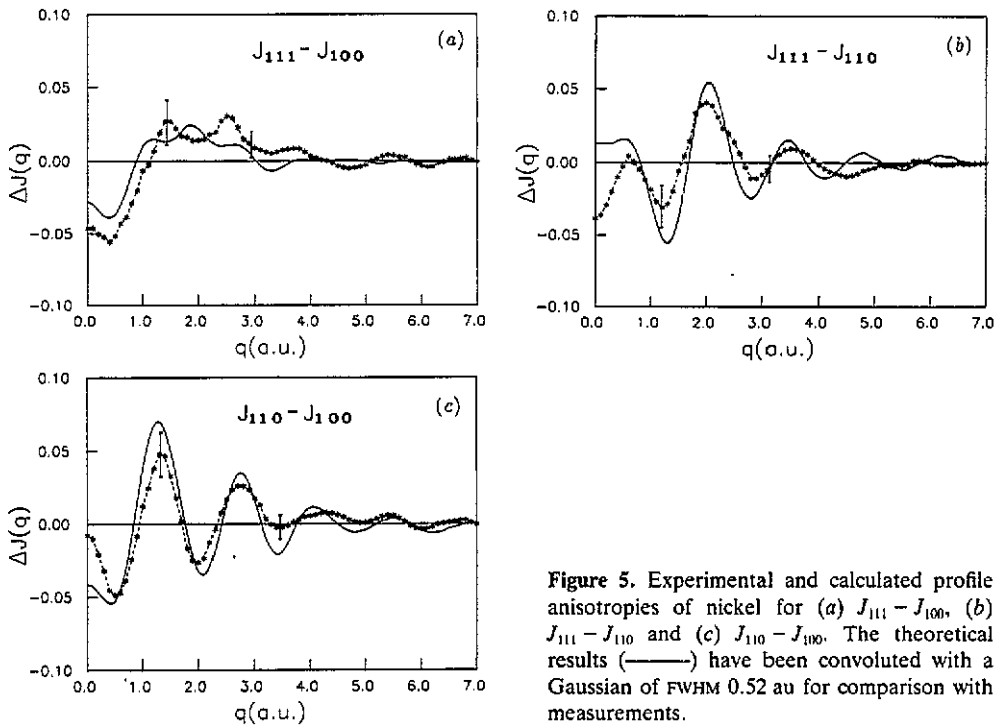
Figure 5. Experimental and calculated profile anisotropies of nickel for (a) $J_{111} - J_{100}$, (b) $J_{111} - J_{110}$ and (c) $J_{110} - J_{100}$. The theoretical results (———) have been convoluted with a Gaussian of FWHM 0.52 au for comparison with measurements.

not due to other existing Γs projected at the same momentum. Since d states at Γ are *far* from the Fermi level we believe that they would not give any difference between experiment and theory by themselves and, in any case, they would not explain the main minima in the other directions. However, this information could not have been deduced without a detailed knowledge of the band structure and the EMD.

4.3. Compton profile anisotropy

The experimental and calculated Compton profile anisotropies of Ni (i.e. the differences between pairs of directional profiles) are plotted in figure 5. The theoretical results (full curves) have been convoluted with a Gaussian of 0.52 au FWHM to account for the experimental resolution function. The interpretation of Compton scattering data in this form has the advantage of elimination of residual systematic errors.

There is generally good agreement between theory and experiment in the position of the various oscillations derived from the Fermi surface geometry. For the two differences $J_{111} - J_{110}$ (figure 5(b)) and $J_{110} - J_{100}$ (figure 5(c)) the calculation predicts anisotropies of 0.11 electrons au^{-1} and 0.13 electrons au^{-1} which are larger than the experimental values of 0.075 electrons au^{-1} and 0.10 electrons au^{-1}, respectively. This is consistent with the analysis of Rollason *et al* [5], who attribute this discrepancy to non-local correlation effects. For these two differences there is a remarkable agreement between the present experimental anisotropies and those of earlier measurements [4, 5], despite the different resolutions. The theoretical difference $J_{111} - J_{100}$ (figure 5(a)) has the same behaviour as the experimental one with a slightly smaller amplitude of oscillations. It is

also found that, between 1 and 3 au, J_{111} is larger than J_{100}, while the experiment [5] using an Au source showed no significant difference between these two directions.

Our theoretical results also agree well with the earlier LCGO band-structure calculation [8, 25] in regard to the main features and positions of the anisotropies. Our magnitudes, however, are typically within our experimental error margins, whereas those based on Gaussian-type orbitals typically differ by as much as 1.5 times [8] to twice [25] our experimental error margins. This can be attributed to the wider conduction bands of the methods using atomic orbitals than those of APW with Hedin and Lundqvist exchange and correlation [26]. If their unoccupied states are higher in energy than ours, then their Fermi cut would be closer to Γ, especially in the $\langle 110 \rangle$ directions where the d band is monotonic, and the Fermi surface would be more compressed, especially in the $\langle 110 \rangle$ directions. This would result in larger CP anisotropies than ours near the positions of the Fermi breaks, as is actually observed, even at small momenta where the d contribution to the EMD is still small.

Incidentally this would explain also the main differences between our figures 4 and the relevant figures in [5], which display the differences between the corresponding experimental and theoretical CPs. Near the first Fermi cut they find a maximum, whereas we do not find any substantial difference, and their maxima at subsequent Fermi cuts in the repeated zone scheme are slightly wider than ours. With the Fermi cuts closer to Γ the LCGO treatment would leave more (wider) unoccupied momentum space than our APW treatment would do.

5. Conclusions

We have presented an experimental and theoretical study of the EMD for nickel. The Compton scattering measurements were carried out using 60 keV γ-rays on single-crystal samples of nickel. Although a Au spectrometer has a better detector resolution, we find that an Am spectrometer with a very well fixed scattering vector can be used equally well, if not better than in [5], to obtain absolute CPs. Our calculations of the EMD and Compton profile are based on the self-consistent APW method, using the local-density approximation of Hedin and Lundqvist.

The general shape of the theoretical momentum density for Ni, together with its various features and Fermi breaks have been analysed in terms of the corresponding energy bands, the Fermi surface topology and the character of the wavefunctions. A comparison has been performed between the experimental and calculated absolute Compton profiles, showing that the correlation correction term improves their agreement near $q = 0$. At higher momenta there are maximum discrepancies between theory and experiment of about 2% $J(0)$, which reveal the appearance of non-local correlation effects.

Concerning the profile anisotropies there is a good agreement between calculation and measurements in the position of the oscillations, but the theoretical anisotropies $J_{110} - J_{100}$ and $J_{111} - J_{110}$ are larger than the experimental anisotropies, a feature which has also been found for other transition metals, such as Cu [17], V and Nb [19].

References

[1] Williams B G (ed) 1977 *Compton Scattering* (New York: McGraw-Hill)
[2] Suzuki K and Itoh F 1981 *Progress in the Study of Application of Electron Theory to Materials Science* ed M Doyama (Tokyo: University of Tokyo) p 258
[3] Williams B G and Thomas J M 1983 *Int. Rev. Phys. Chem.* 3 39
Cooper M J 1985 *Rep. Prog. Phys.* 48 415
[4] Eisenberger P and Reed W A 1974 *Phys. Rev.* B 9 3242
[5] Rollason A J, Schneider J R, Laundy D S, Holt R S and Cooper M J 1987 *J. Phys. F: Met. Phys.* 17 1105
[6] Hedin L and Lundqvist B I 1971 *J. Phys. C: Solid State Phys.* 4 2064
[7] Lam L and Platzman P M 1974 *Phys. Rev.* B 9 5122
[8] Wang C S and Callaway J 1975 *Phys. Rev.* B 11 2417
[9] Holt R S and Cooper M J 1983 *Nucl. Instrum. Methods* 213 447
Cooper M J 1987 *J. Physique Coll.* C9 989
[10] Manninen S and Paakkari T 1978 *Nucl. Instrum. Methods* 155 115
[11] Halonen V, Williams B G and Paakkari T 1975 *Phys. Fenn.* 10 107
Williams B G and Halonen V 1975 *Phys. Fenn.* 10 5
Halonen V and Williams B 1979 *Phys. Rev.* B 19 1990
[12] Cardwell D A and Cooper M J 1986 *Phil. Mag.* B 54 37
[13] Anastassopoulos D L and Priftis G D 1991 unpublished
[14] Bacalis N C, Papanicolaou N I and Papaconstantopoulos D A 1986 *J. Phys. F: Met. Phys.* 16 1471
Papanicolaou N I, Bacalis N C and Papaconstantopoulos D A 1988 *Phys. Rev.* B 37 8627
[15] Mattheiss L F, Wood J H and Switendick A C 1968 *Methods Comput. Phys.* 8 63
[16] Platzman P M and Tzoar N 1965 *Phys. Rev.* 139 A410
Eisenberger P and Platzman P M 1970 *Phys. Rev.* A 2 415
[17] Bauer G E W and Schneider J R 1984 *Phys. Rev. Lett.* 52 2061; 1985 *Phys. Rev.* B 31 681
Pattison P, Hansen N K and Schneider J R 1982 *Z. Phys.* B 46 285
[18] Lundqvist B I 1968 *Phys. Kondens. Mater.* 7 117
[19] Papanicolaou N I, Bacalis N C and Papaconstantopoulos D A 1987 *Z. Phys.* B 65 453
[20] Harthoorn R and Mijnarends P E 1978 *J. Phys. F: Met. Phys.* 8 1147
[21] Kanhere D G and Singru R M 1977 *J. Phys. F: Met. Phys.* 7 2603
[22] Hubbard J 1969 *J. Phys. C: Solid State Phys.* 2 1222
[23] Mijnarends P E 1973 *Physica* 63 235
[24] Biggs F, Mendelsohn L B and Mann J B 1975 *At. Data Nucl. Data Tables* 16 201
[25] Sundararajan V, Asokamani R and Kanhere D G 1988 *Phys. Rev.* B 38 12653
[26] Bacalis N C, Papaconstantopoulos D A and Pickett W E 1988 *Phys. Rev.* B 38 6218